Original Research

Aortic Flow Patterns After Simulated Implantation of Transcatheter Aortic Valves

Anastasios Kopanidis[1,2], Ioannis Pantos[2,3], Nikolaos Alexopoulos[2], Andreas Theodorakakos[4], Efstathios Efstathopoulos[3], Demosthenes Katritsis[2,5]

[1]Department of Mechanical Engineering, University of Western Macedonia, Kozani, [2]Department of Cardiology, Athens Euroclinic, [3]Second Department of Radiology, Medical School, National and Kapodistrian University of Athens, [4]Department of Mechanical Engineering, Technological Education Institute of Piraeus, Egaleo, Greece; [5]Beth Israel Deaconess Medical Center, Harvard Medical School, Boston, MA, USA

Key words:
Bioprosthetic valves, aortic flow, computational fluid dynamics.

Introduction: The functional behavior and hemodynamic characteristics of percutaneously implanted bioprosthetic valves are not known.

Methods: We created aortic models after the simulated implantation of two of the most widely used bioprosthetic valves: the Edwards SAPIEN, and the Medtronic CoreValve. By using computational fluid dynamics analysis we sought to investigate variations in the aortic flow patterns induced by the two valve designs and their association with detrimental phenomena such as vascular remodeling, vascular wall damage and thrombosis.

Results: The simulated implantation of models that resemble the two valves resulted in different aortic flow conditions. Vortex formation in the upper ascending aorta was more persistent in the case of the simulated Medtronic valve. The ranges of average wall shear stress (WSS) values were 2.4-3.5 Pa for Edwards and 3.0-5.3 Pa for Medtronic; the calculated WSS values induced endothelial quiescence and an atheroprotective setting in both valves. The average shear stress on the simulated valve leaflets was low; however, hotspots were present in both valves (155.0 Pa for Edwards and 250.0 Pa for Medtronic) which would in theory be able to cause platelet activation and thus promote thrombosis. The pressure drops along the aorta were slightly lower for the Edwards compared to the Medtronic valve (198.0 Pa versus 218.0 Pa).

Conclusions: The presented method allows the assessment of aortic flow conditions following the implantation of bioprosthetic valves. It may be useful in predicting detrimental flow phenomena, thus facilitating the selection of appropriate valve designs.

Manuscript received:
September 17, 2014;
Accepted:
June 15, 2015.

Address:
Demosthenes Katritsis

Department of Cardiology
Athens Euroclinic,
9 Athanassiadou St.
115 21 Athens, Greece
dkatritsis@euroclinic.gr,
dkatrits@bidmc.harvard.edu

Aortic stenosis (AS) is one of the most prevalent forms of cardiovascular disease in the Western world and represents the most common form of valvular heart disease requiring surgery in Europe.[1,2] Percutaneous implantation of bioprosthetic valves through a transfemoral, subclavian, transaortic, or transapical route is evolving fast, with promising results in inoperable or high-risk patients.[3-10] Although several valves are under study, the most widely used types so far are the Edwards SAPIEN valve system (Edwards Lifesciences Inc., Irvine, CA), which is a trileaflet bovine pericardial valve mounted on a cobalt chromium stent frame, and the CoreValve system (Medtronic, Minneapolis, MN), which is a trileaflet porcine pericardial valve mounted on a self-expanding nitinol stent (Figure 1).[5-9,11,12] In-hospital mortality and procedural complications such as embolic stroke do not differ significantly between the SAPIEN and CoreValve.[5-9,11] Significant atrial regurgitation (AR; grade ≥3) and the need for permanent pacing are more common with the CoreValve than with the SAPIEN, whereas coronary artery occlusion is more com-

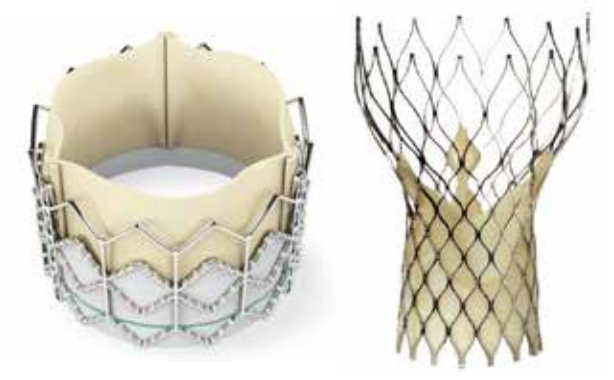

Figure 1. Illustration of the Edwards SAPIEN (left) and Medtronic CoreValve (right) transcatheter aortic valves, which were simulated and virtually implanted in a representative aortic model.

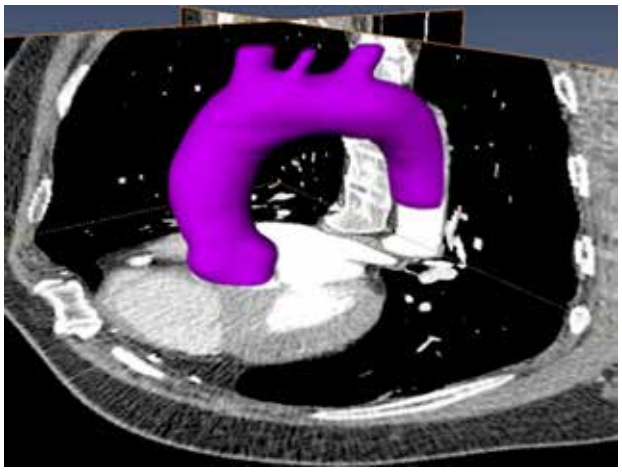

Figure 2. The 3-D surface of the representative aortic model (colored surface) and the corresponding computed tomography coronary angiography images from which the aortic model was derived.

mon with the SAPIEN, occurring mainly in patients with a lower lying coronary ostium and shallow sinuses of Valsalva.[8] Although most of these differences can be attributed to structural characteristics or scaffolding properties, the functional behavior and hemodynamic characteristics of these particular valves are not known, and no *in vivo* or *in vitro* data exist in this regard. However, aortic flow conditions are associated with vascular remodeling, vascular wall damage and thrombosis, and aneurysm formation. Computational fluid dynamics provide the opportunity to assess flow characteristics using representative theoretical models.[4,13,14]

The purpose of the present study, therefore, was to apply computational fluid dynamics analysis in order to compare the hemodynamic characteristics of the CoreValve and SAPIEN systems. We considered an aortic model free of pathologies, derived from computed tomography coronary angiography (CTCA), and created aortic models that incorporated the bioprosthetic valves. By applying the same inflow and outflow boundary conditions, we sought to investigate variations in the aortic flow patterns induced by the two valve designs and their association with detrimental phenomena such as vascular remodeling, vascular wall damage and thrombosis.

Methods

Simulation of aortic flow with the two virtually implanted bioprosthetic valves was accomplished through the following steps: (i) acquisition of a realistic model of the aorta; (ii) simulation of the shape of each valve at each operation phase; (iii) merging of the simulated valves with the aortic model; and (iv) definition of inflow and outflow boundary conditions in the combined aortic model, considering blood as a Newtonian fluid.

Aortic model construction

A typical aortic geometry was obtained by CTCA from a patient without any aortic pathology. The CTCA examination was performed using a 128-slice CT scanner (Aquilion CX, Toshiba, Tokyo, Japan) with a slice thickness of 0.5 mm. We considered axial CTCA slices of the opacified aortic lumen of the ascending aorta, starting at the sinus of Valsalva, the aortic arch, the descending aorta and the lower segments of the brachiocephalic artery, left common carotid artery, and left subclavian artery. These slices were fed into a commercially available software package (Amira 4.0, Mercury Computer Systems). The lumen of the aorta and branches were semi-automatically segmented with the aid of an experienced radiologist, using tools provided by the software package. A total of 360 slices were processed from the patient CT data. The 3-D surface model of the aorta and branches was generated automatically and semi-automated filtering was applied to reduce the fine-scale irregularities of the surface model. Figure 2 shows the 3-D surface model of the aorta and corresponding CTCA images.

Valve construction

We considered two valves that are currently in widespread use: the balloon-expanded Edwards SAPIEN

XT (Edwards Lifesciences, Irvine, CA, USA) and the self-expanding CoreValve (Medtronic Inc., Minneapolis, MN, USA) (Figure 1). The virtual construction of the two valves was accomplished by following the dimensions provided by the manufacturers, published data from relevant studies,[15,16] and adopting simplified topologies of the two valves on a commercial computer-aided design system (SolidWorks 2010, SolidWorks Corp., Concord, MA, USA). The shape of both simulated valves followed closely the original shape, which was defined by the strut scaffold. Nominal dimensions for both valves followed those of the 29 mm diameter models. Each valve was modeled in three distinct phases of its operation, with varying valve openings of 1/3, 2/3 and 3/3 (fully opened valve) of the total surface area. For both valves, the metal struts of the supporting stent were omitted and only the moving leaflets were constructed for each simulated operation phase. The morphology of the leaflets was also in accordance with literature reports and manufacturers' data and represented the topology of the leaflets in the three distinct phases of the valve's operation. In the case of the Medtronic CoreValve, data were also extracted via direct measurements on an available functional valve. We used a scallop shape for the leaflet geometry design and mounted the leaflets on a rigid straight tube in the case of Edwards and on a rigid converging–diverging tube in the case of Medtronic (Figures 3 and 4).

Valve implementation in the aortic model and mesh generation

The three generated models for each valve were incorporated into the model of the acquired aorta, first by aligning the axis of the valve to that of the aorta at the plane of the sinuses of Valsalva, and then by adjusting the plane of the closed leaflets of the simulated valve to that of the bottommost of the Valsalva sinuses. After the construction of the computational domain topology had been completed, a numerical computation mesh was applied, with the use of a commercial package (ANSYS). Hybrid volume elements of the same element size (2.7×10^{-5} m) were used for all cases, resulting in mesh sizes between 1.2×10^{6} and 2.0×10^{6} elements. Mesh independence analysis involved 3 different sizes of mesh (1.6×10^{5}, 1.8×10^{6}, and 4.0×10^{6}). The differences in pressure drop results between the middle mesh sizes were 3.5% and 5.5% for the two extreme cases, respectively, leading to the choice of the aforementioned element size.

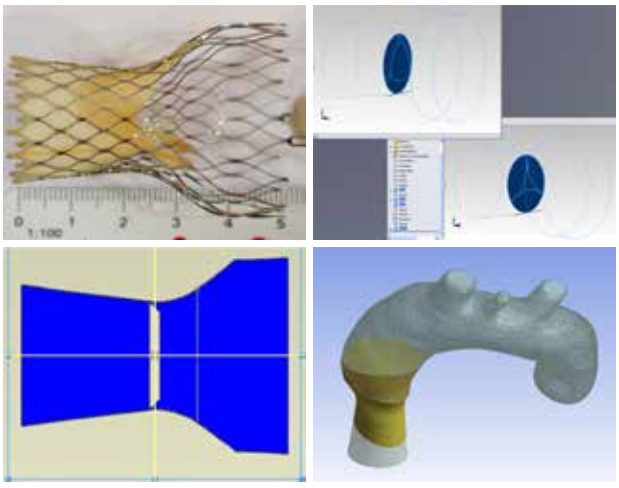

Figure 3. Construction of the virtual model of the Medtronic CoreValve and integration into the aortic model. In this case both published data and an actual valve were available and were used in the modeling of the virtual valve.

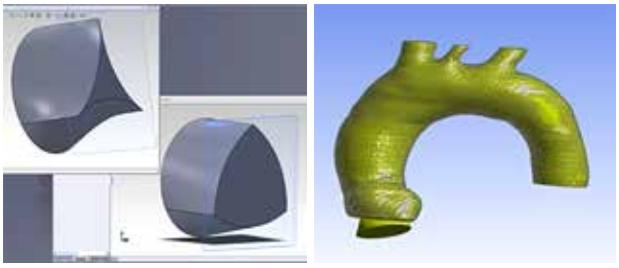

Figure 4. Construction of the virtual model of the Edwards SAPIEN and integration into the aortic model. In this case all information regarding the valve was acquired from data provided by the manufacturer and from the relevant literature.

Flow simulation

All simulated cases were approached using a steady-state computational fluid dynamics iterative methodology in the sense of "freezing" the time and investigating the flow field for each "snapshot" of the considered valves' operation phases. No turbulence model was used, as flow was considered laminar. The Reynolds number varied from 1808 to 4820 for flow in a cylinder, calculated using the valve's entry diameter. Even though flow in a pipe considers flows with Re>4000 to be in the turbulence range, this was exceeded only locally and when a k-ε model was used, convergence issues made the solution unreliable. The same happened when a shear-stress transport model was used for the case of Re=4820; therefore, the original flow field approach with laminar parameters was retained for the solution. All cases converged after 2000 iterations or

earlier. Boundary conditions in all cases involved blood mass inflow according to the area of the opened valve, as defined by the shape of the open valve leaflets for each considered operation phase. Blood mass flow conditions during the cardiac cycle were adopted from a previous relevant study, which acquired flow velocity and flow rate waveforms *in vivo* by phase contrast magnetic resonance imaging.[4] A quasi-static approach was used to analyze aortic flow at the various instances of valve operation.[16] Outflow mass fraction for each outlet was defined according to Murray's law, which suggests that the flow ratio through a main vessel and a bifurcation is proportional to the inverse ratio of their diameters raised to the third power.[17] Table 1 tabulates inflow values and outflow percentages for each simulated case. Blood was assumed to be a Newtonian and incompressible fluid with dynamic viscosity of 3.50 mPa·s and a density of 1060 kg/m^3.[18]

Table 1. Boundary inflow and outflow conditions for the simulated valves and operation phases.

		Mass outflow fraction per outlet			
Simulated case	Mass inflow (kg/s)	BCA	LCCA	LSA	DESC
Edwards 1/3	0.195				
Edwards 2/3	0.311				
Edwards 3/3	0.384	10.7%	4.0%	7.0%	78.3%
Medtronic 1/3	0.144				
Medtronic 2/3	0.212				
Medtronic 3/3	0.384				

BCA – brachiocephalic artery; LCCA – left common carotid artery; LSA – left subclavian artery; DESC – descending aorta.

Flow parameters

We assessed flow parameters that are considered relevant to flow-induced detrimental phenomena, such as thrombosis, vascular wall damage, and valve failure, and we also considered the impact of valve implantation on myocardial load. We assessed both qualitative and quantitative flow parameters; the former include the visualization of flow path lines by streamtrace tracking of free particles released at the inflow in order to assess flowing velocity, vortex formation and flow recirculation, and the latter include the calculation of shear stress, the shearing force exerted on the vessel walls and valve leaflets due to the flowing blood. We also considered blood pressures and pressure drops along the flow domain in order to evaluate the efficiency of the implanted valve regarding induced myocardial load. Although we cannot directly link flow parameters and implantation outcome, it is plausible that the risk of thrombosis, vascular damage or valve failure would be higher if regions of the aorta are continuously exposed to flow conditions that promote these detrimental phenomena.

Results

The complex, time-dependent, three-dimensional nature of the aortic flow field makes its presentation challenging. To illustrate the intricate dynamics of the flow field, flow trajectories are presented in Figure 5, wall shear stress distributions in Figure 6, and shear stress distributions at the valves' leaflets in Figure 7. These figures clearly demonstrate that the implantation of the two simulated valves and also each simulated phase of valve opening have distinct impacts on the aortic flow conditions. This is reflected in both the distribution and the magnitude of the flow indices in the aortic region.

Flow velocities and flow recirculation

In the case of the 1/3 valve opening, high flow velocities are evident at longer distances from the valve's exit along the ascending aorta for the Medtronic valve (Figure 5). As a result, blood flow impacts the vessel wall of the ascending aorta with higher velocity and a flow vortex is subsequently formed at the aortic arch between the brachiocephalic and left common carotid branches (red arrow). Such a vortex is not evident in the case of the Edwards valve. This is likely due to the different geometries of the two valves. Medtronic's flow exit is slightly higher (upstream) in comparison to the Edwards' flow exit; thus, in the case of the Medtronic valve the flow enters a region of vessel curvature (aortic arch) and branching (brachiocephalic and carotid branches) at higher velocities. The flow conditions at 2/3 valve opening are similar for both valves, although now considerably lower flow velocities are evident in the whole flow domain (ascending aorta, aortic arch and descending aorta). The flow vortex that was formed in the case of the Medtronic valve during the earlier phase of valve opening is still evident (green arrow); however, the recirculation velocity is now lower and significantly fewer particles participate in the vortex, indicating that forward flow is gradually restored. In the case of the Edwards valve, a small but identifiable vortex is formed

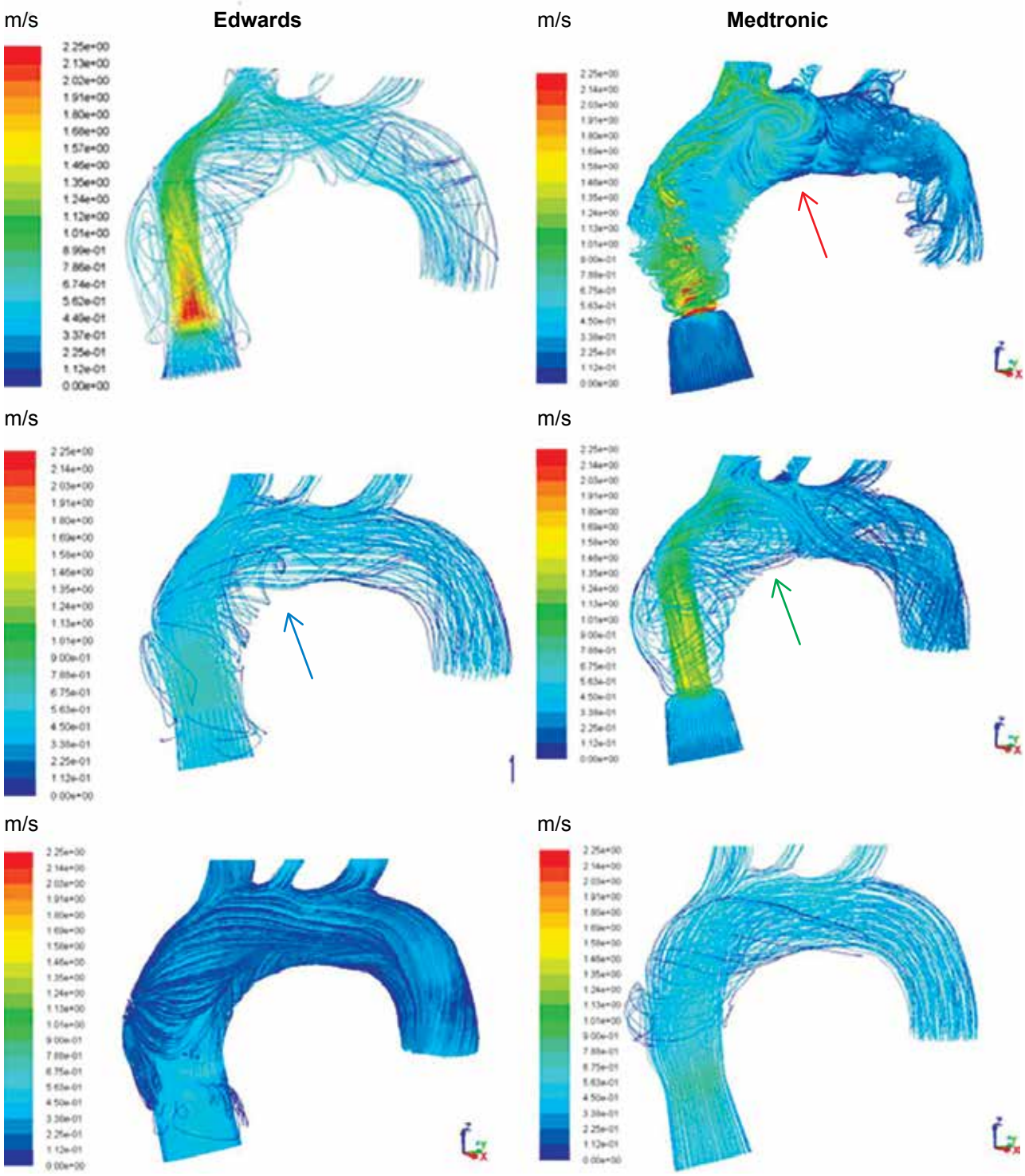

Figure 5. Pathlines and velocity magnitude of blood flow for the simulated Edwards valve (left panel) and Medtronic valve (right panel) at the three considered phases of valve opening (1/3 upper row, 2/3 middle row and 3/3 lower row).

at this instant (blue arrow), which was not previously present. The flow conditions at 3/3 are considerably smoother for both valves, with absence of any flow recirculation and the majority of particles participating in forward flow, with overall lower flow velocities compared to the previous phases.

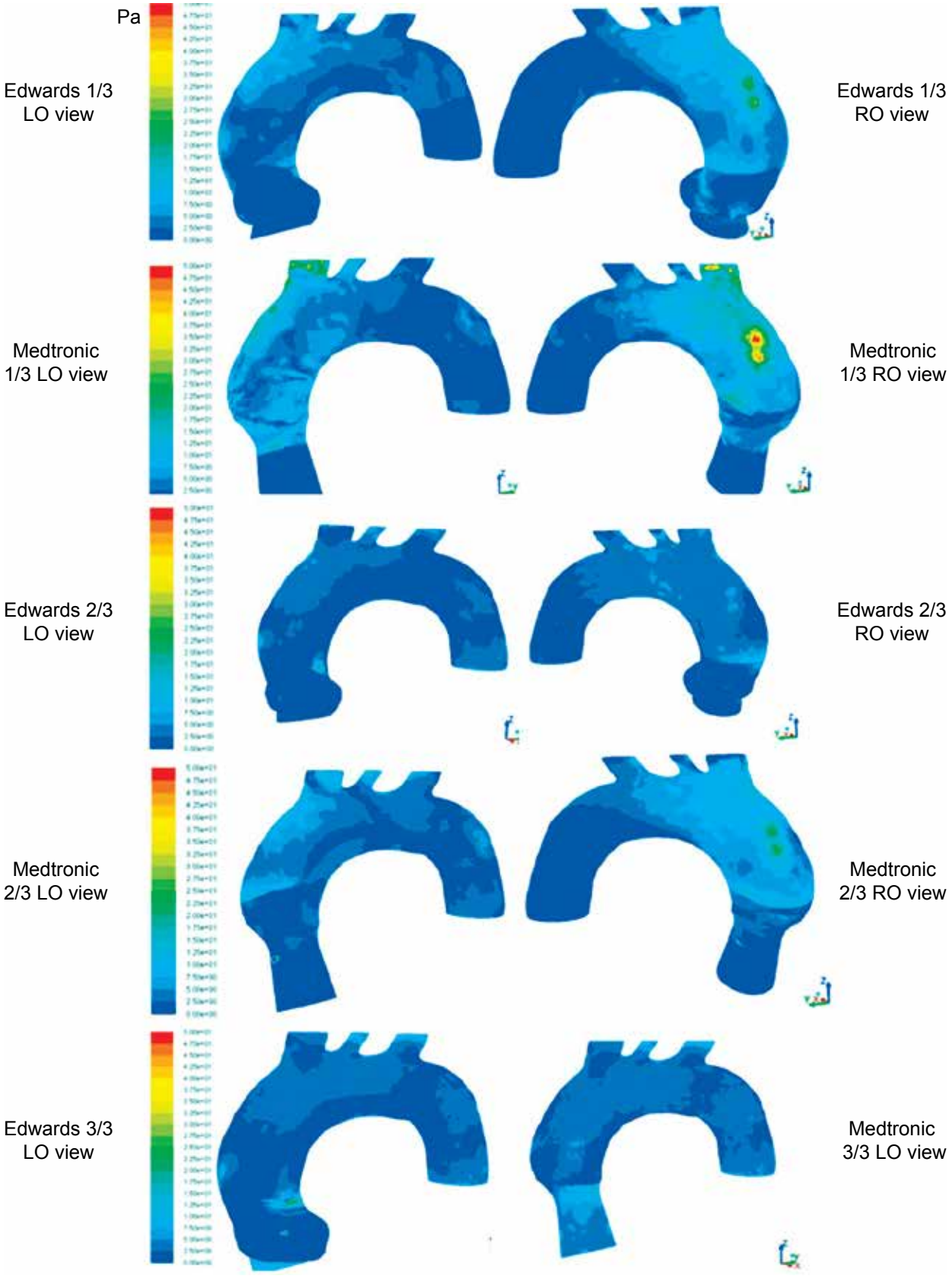

Figure 6. Wall shear stress (WSS) distribution for the simulated Edwards valve and Medtronic valve at the three considered phases of valve opening. WSS distributions are presented for both the left-oblique (LO) and right-oblique (RO) views of the aorta.

Wall shear stress

The distributions of WSS in the aorta are similar for the two simulated valves: at the 1/3 valve opening higher WSS values are evident in the outer walls of the aorta, "opposite" the valve opening, and lower WSS at the inner curve of the aortic arch and the descending aorta (Figure 6). Two "hotspots" of high WSS values are seen for both valves in the ascending aorta below the brachiocephalic branch; these are due to high-velocity particles in the central axis of the aorta, which impact on the artery walls. The distributions of WSS in the aorta are more uniform in the phase of 2/3 valve opening and overall lower WSS are evident; however, in the case of the simulated Medtronic valve the two "hotspots" of high WSS are still identifiable. In the phase with a fully open valve, the distributions of WSS in the aorta are very similar for both valves, with a uniform distribution of WSS values and absence of any distinct characteristics. The average values of WSS calculated for the whole aortic model are generally higher for the simulated Medtronic valve for all operation phases (Table 2). The maximum differences were noted for the 1/3 and 2/3 valve opening phases, where the average WSS values for the Medtronic valve were 1.5-fold higher.

Leaflet shear stress

The average shearing stresses that were exerted on the leaflets of the two simulated valves were in the range 1.8-15.2 Pa (Table 2). The highest shear stress values were evident at the edges of the leaflets for both valves, as the greatest flow velocity gradients were at these points (Figure 7). In the case of the simulated Medtronic valve, "hotspots" of shear stress were also seen at the periphery of the valve in the phase of 2/3 opening. In the case of fully open valves (3/3), the highest shear stress values were distributed differently between the two valves: for the Edwards valve, the highest shear stress values of 15.0 Pa were evident at the bottom of the valve, whereas for the Medtronic valve the highest shear stress values of 22.0 Pa were distributed in the central part of the valve.

Pressure drop

The pressure drop or pressure gradient along a vessel can be viewed as the force that drives blood flow. Thus, a low pressure drop indicates that the energy that has to be supplied by the myocardium to drive this flow is low, and low pressure drops are therefore considered beneficial in terms of myocardial load (Table 3). For all considered vessels, pressure drops were lower for the simulated Edwards valve than for the Medtronic valve. The highest pressure drops were evident between the ascending and descending aorta (198.0 Pa and 218. 0 Pa for Edwards and Medtronic, respectively). The differences in pressure drop between the two simulated valves were 9% for the descending aorta, 21% for the brachiocephalic artery, 6% for the left common carotid artery, and 7% for the left subclavian artery.

Table 2. Average wall shear stress (WSS) and maximum leaflet shear stress (SS) for the simulated valves and operation phases.

Simulated case	WSS (Pa)	Leaflet SS (Pa)
Edwards 1/3	3.5	5.3
Edwards 2/3	2.5	2.1
Edwards 3/3	2.4	5.5
Medtronic 1/3	5.3	15.2
Medtronic 2/3	3.7	1.8
Medtronic 3/3	3.0	3.1

Discussion

Although the percutaneous implantation of bioprosthetic valves is promising, the clinical value of this approach is still under study. The reported one-year mortality after transcatheter aortic valve replacement is 20%, similar to that of high-risk patients who undergo surgical valve replacement (18%).[5-7,9,11,19] Two-year mortality is rather similar (33.9% vs. 35%),[4] and long-term results (5 years) have detected a valve failure rate of 3.4%.[20] The technical characteristics of the implanted valve may be of importance in this respect. A plausible influence on implantation outcome is the aortic flow setting induced by the bioprosthetic valve, since aortic flow conditions are associated with various detrimental phenomena, such as vascular remodeling, vascular wall damage and thrombosis. Although the genesis of aortic aneurysms can be explained in many ways,[21] recent evidence indicates that flow dynamics (turbulence or stagnation) may in fact stress vessel walls, affecting the development of aortic aneurysms.[22,23] The WSS reflects the shear stress of fluid against the vascular wall or the viscous drag of blood.[24] This force is minimal (1-20 Pa) compared with arterial blood pressure (100 mmHg ≈13000 Pa), however endothelial cells are responsive to variations in WSS.[25] Such changes have a strong link with the onset and development of atherosclerosis, and possi-

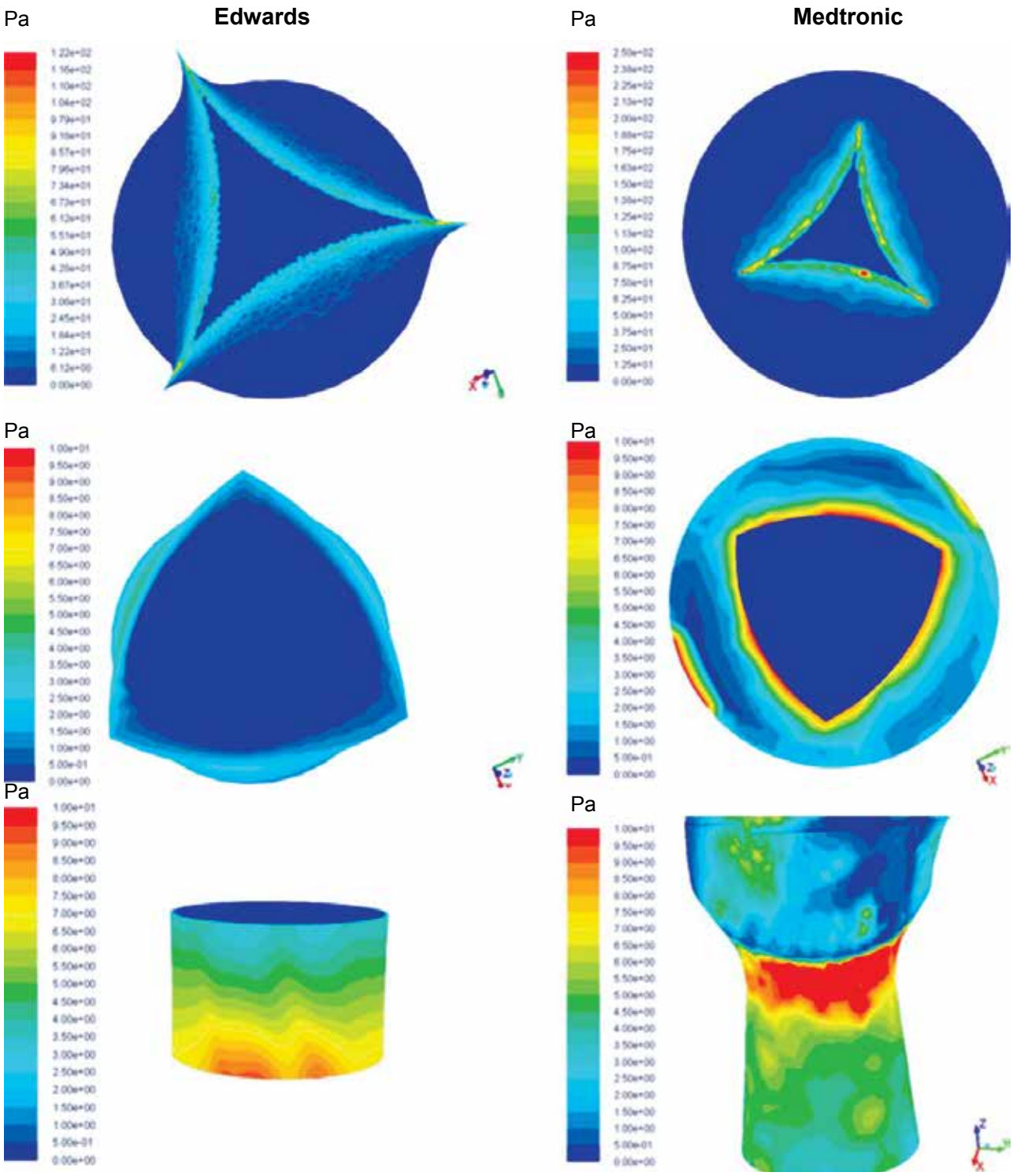

Figure 7. Shear stress distribution at the valve leaflets for the simulated Edwards valve (left panel) and Medtronic valve (right panel) at the three considered phases of valve opening (1/3 upper row, 2/3 middle row and 3/3 lower row).

bly the occurrence of aneurysms. This study sought to comparatively evaluate post-implantation aortic flow conditions with two popular bioprosthetic valves, using computational flow dynamics to simulate aortic flow.

The aortic flow patterns induced by the two valves were generally similar; however, several variations were also identifiable. These variations were due to the different geometries and design modules of the

Table 3. Pressure drop between the ascending aorta and the descending aorta and branches.

Simulated case	Pressure drop per outlet (Pa)			
	BCA	LCCA	LSA	DESC
Edwards 3/3	66.0	163.0	153.0	198.0
Medtronic 3/3	84.0	172.0	165.0	218.0

Abbreviations as in Table 1.

valves. The Medtronic valve has a taller profile and the valve's outlet is slightly upstream in comparison to the Edwards valve, although both valves were virtually implanted so as to have the transverse plane defined by the closed valve leaflets at the same location. This geometric variation, in combination with the higher outflow velocities for the simulated Medtronic valve, leaves less room for smooth flow development before flow enters the curved section of the aorta, resulting in the formation of a larger and more persistent flow vortex. Thus, a shorter valve profile appears theoretically advantageous. A transvalvular jet was suggested as one of the important factors contributing to aneurysmal dilatation of the thoracic aorta, by regulating the matrix metalloproteinase level in the wall tissue.[26] Similarly to our findings, a previous MRI study in patients who underwent implantation of an Edwards SAPIEN valve revealed asymmetrical systolic left ventricular outflow, with a flow jet forming along the right anterior outer curvature of the ascending aorta that caused the development of marked helical flow.[27] These findings are of particular interest in light of a recent study in high-risk patients with severe aortic stenosis, which showed that transcatheter replacement resulted in much more frequent perivalvular aortic regurgitation, possibly related to a less seamless alignment of the transcatheter prosthesis compared with surgically repaired valves.[28]

The WSS distribution following transcatheter aortic valve implantation is also of interest, since it may affect the endothelial and biological functions of the aorta. In this study, the highest WSS values for both valves were noted at the aortic arches. Our results are in keeping with those of a previous study that compared ascending aortic flow and WSS patterns in bicuspid and tricuspid aortic valves and found that the maximum WSS values were localized around the mid-ascending aorta level, highlighting the effect of the jet flow on this portion of the wall.[29] Our results regarding average WSS values are higher than those of relevant previous studies that calculated average WSS at a level of less than 1.0 Pa.[4,22,30] However those studies calculated the time-averaged WSS throughout the cardiac cycle; thus, they also considered time intervals during valve closing when there was a reduced blood flow and thus reduced WSS values, whereas in our study we considered three distinct time points during valve opening, all with considerable blood flow rates. Nevertheless, the calculated average WSS values in our study are in a range that induces endothelial quiescence and an atheroprotective gene expression profile,[31] but not high enough to cause matrix degradation in the wall, with the possible consequence of local enlargement and aneurysm.[32]

Previous experimental and numerical blood studies have shown that high shear stress levels cause platelet activation, while long exposure times to these shear stresses combined with flow recirculation promote thromboembolism.[33] Similarly to a previous study,[34] we have demonstrated that the WSS increases gradually from the base of the leaflet toward the tip, and reaches its peak at the edge of the leaflet tip, where the maximum axial flow acceleration occurs. Additionally, the WSS distributions presented in this study clearly showed complex stress development patterns during the opening of the valve, which is considered to be the most detrimental factor for fatigue failure analysis.[34] Platelet activation is pronounced at the region of the bioprosthetic valve, owing to the complex flow conditions that the blood experiences at this region.[35,36] Activated platelets with a long residence time in these flow regions may aggregate, leading to the formation of free emboli.[37] We were not able to gain insight into platelet activation, since this requires assessing the trajectories of particles and the duration of exposure to elevated shear stresses throughout the cardiac cycle. However, very high shear rates in the order of 10,000 s^{-1}, which correspond to shear stresses of 35 Pa, may cause immediate platelet activation.[38] Although the average leaflet shear stresses calculated in this study were considerably lower for both valves, there were some "hotspots", at which shear stress was higher than 35 Pa, for both simulated valves.

Our study demonstrated that the virtual implantation of bioprosthetic aortic valves and the prediction of post-implantation aortic flow patterns by computational methodologies are feasible. Previous studies have also used computational methods to simulate implant deployment, in order to select the appropriate implant size and type,[39] or to model the interac-

tion between the device and the aortic root anatomy, in order to study device performance.[40] Therefore, such computational methodologies can theoretically be jointly applied in preoperative planning to assess the structural, functional and rheological outcome of implantation with a view to the selection of the most appropriate valve system.

Our study has several limitations. We considered an aortic model from a normal subject in which the bioprosthetic valves were incorporated, instead of directly reconstructing the anatomy of patients with implanted valves. However, this approach allowed a direct comparison of the flow variations induced by the valve design. Inflow boundary conditions were not acquired from the same subject from whom the vessel model was acquired. Although this would not be expected to influence the distribution of flow indices at the aorta, it could have a significant impact on their absolute values. As in most relevant studies, the aortic wall was assumed to be rigid and fixed, with no radial expansion or translational motion; however, the effect of this assumption is likely to be insignificant.[41,42] A quasi-static approach was considered, rather than pulsatile flow conditions; however, at each phase of the simulated valve operation we considered varying inflow conditions according to the phases of valve opening. The arterial model that we considered was taken from a normal subject; therefore, simulation results would be different in the case of aortic pathologies, such as aortic dilation or constriction. The simulated models of the two valves closely resemble the geometry and dimensions of the actual valves; however, they cannot be considered as exact reproductions. Since the metal struts of the supporting stent were omitted, their impact on the WSS distribution was not considered.[15,16] Finally, we assumed an ideal valve configuration after implantation and non-compliant valve geometries;[16] however, during implantation of transcatheter aortic valves into calcified aortic annuli, misdeployment is likely, given the asymmetric shape of the target region.[43]

Conclusions

Acknowledging the various limitations, our study demonstrates that aortic flow conditions after the simulated implantation of transcatheter aortic valves can be assessed using computational fluid dynamics. This methodology may be of value in the selection of appropriate valve systems and the future design of prosthetic valves, for either surgical or transcatheter implantation.

Acknowledgments

This work was supported by a grant from the S. Niarchos Foundation.

References

1. Maganti K, Rigolin VH, Sarano ME, Bonow RO. Valvular heart disease: diagnosis and management. Mayo Clin Proc. 2010; 85: 483-500.
2. Dweck MR, Boon NA, Newby DE. Calcific aortic stenosis: a disease of the valve and the myocardium. J Am Coll Cardiol. 2012; 60: 1854-1863.
3. Makkar RR, Fontana GP, Jilaihawi H, et al. Transcatheter aortic-valve replacement for inoperable severe aortic stenosis. N Engl J Med. 2012; 366: 1696-1704.
4. Kodali SK, Williams MR, Smith CR, et al. Two-year outcomes after transcatheter or surgical aortic-valve replacement. N Engl J Med. 2012; 366: 1686-1695.
5. Chieffo A, Buchanan GL, Van Mieghem NM, et al. Transcatheter aortic valve implantation with the Edwards SAPIEN versus the Medtronic CoreValve Revalving system devices: a multicenter collaborative study: the PRAGMATIC Plus Initiative (Pooled-RotterdAm-Milano-Toulouse In Collaboration). J Am Coll Cardiol. 2013; 61: 830-836.
6. Jilaihawi H, Chakravarty T, Weiss RE, Fontana GP, Forrester J, Makkar RR. Meta-analysis of complications in aortic valve replacement: comparison of Medtronic-Corevalve, Edwards-Sapien and surgical aortic valve replacement in 8,536 patients. Catheter Cardiovasc Interv. 2012; 80: 128-138.
7. Khatri, P, Webb, J, Rodés-Cabau, J et al. Adverse effects associated with transcatheter aortic valve implantation: a meta-analysis of contemporary studies. Ann Intern Med. 2013 158: 35-46.
8. Ribeiro HB, Webb JG, Makkar RR, et al. Predictive factors, management, and clinical outcomes of coronary obstruction following transcatheter aortic valve implantation: insights from a large multicenter registry. J Am Coll Cardiol. 2013; 62: 1552-1562.
9. Généreux P, Head SJ, Hahn R, et al. Paravalvular leak after transcatheter aortic valve replacement: the new Achilles' heel? A comprehensive review of the literature. J Am Coll Cardiol. 2013; 61: 1125-1136.
10. Vavuranakis M, Vrachatis DA, Siasos G, et al. First in Greece transcatheter aortic valve implantation using the CoreValve Evolut-R retrievable and repositionable bioprosthesis with the InLine sheath and the EnVeo Loading guiding catheter: A major advantage for small diameter access vessels. Hellenic J Cardiol. 2015; 56: 338-343.
11. Généreux P, Head SJ, Van Mieghem NM, et al. Clinical outcomes after transcatheter aortic valve replacement using valve academic research consortium definitions: a weighted meta-analysis of 3,519 patients from 16 studies. J Am Coll Cardiol. 2012; 59: 2317-2326.
12. Spargias K, Bouboulis N, Halapas A, et al. Transaortic aortic valve replacement using the Edwards Sapien-XT Valve and the Medtronic CoreValve: initial experience. Hellenic J Cardiol. 2014; 55: 288-293.
13. Sirois E, Sun W. Computational evaluation of platelet activation induced by a bioprosthetic heart valve. Artif Organs. 2011; 35: 157-165.

14. Dwyer HA, Matthews PB, Azadani A, et al. Computational fluid dynamics simulation of transcatheter aortic valve degeneration. Interact Cardiovasc Thorac Surg. 2009; 9: 301-308.
15. Schultz CJ, Weustink A, Piazza N, et al. Geometry and degree of apposition of the CoreValve ReValving system with multislice computed tomography after implantation in patients with aortic stenosis. J Am Coll Cardiol. 2009; 54: 911-918.
16. Sun W, Li K, Sirois E. Simulated elliptical bioprosthetic valve deformation: implications for asymmetric transcatheter valve deployment. J Biomech. 2010; 43: 3085-3090.
17. Reneman RS, Hoeks AP. Wall shear stress as measured in vivo: consequences for the design of the arterial system. Med Biol Eng Comput. 2008; 46: 499-507.
18. Tan FPP, Xu XY, Torii R, et al. Comparison of aortic flow patterns before and after transcatheter aortic valve implantation. Cardiovascular Engineering and Technology. 2012; 3: 123-135.
19. Brennan JM, Edwards FH, Zhao Y, O'Brien SM, Douglas PS, Peterson ED. Long-term survival after aortic valve replacement among high-risk elderly patients in the United States: insights from the Society of Thoracic Surgeons Adult Cardiac Surgery Database, 1991 to 2007. Circulation. 2012; 126: 1621-1629.
20. Toggweiler S, Humphries KH, Lee M, et al. 5-year outcome after transcatheter aortic valve implantation. J Am Coll Cardiol. 2013; 61: 413-419.
21. Kuivaniemi H, Platsoucas CD, Tilson MD 3rd. Aortic aneurysms: an immune disease with a strong genetic component. Circulation. 2008; 117: 242-252.
22. Frydrychowicz A, Stalder AF, Russe MF, et al. Three-dimensional analysis of segmental wall shear stress in the aorta by flow-sensitive four-dimensional-MRI. J Magn Reson Imaging. 2009; 30: 77-84.
23. Xiong J, Wang SM, Zhou W, Wu JG. Measurement and analysis of ultimate mechanical properties, stress-strain curve fit, and elastic modulus formula of human abdominal aortic aneurysm and nonaneurysmal abdominal aorta. J Vasc Surg. 2008; 48: 189-195.
24. Katritsis D, Kaiktsis L, Chaniotis A, Pantos J, Efstathopoulos EP, Marmarelis V. Wall shear stress: theoretical considerations and methods of measurement. Prog Cardiovasc Dis. 2007; 49: 307-329.
25. Hammer S, Jeays A, Allan PL, et al. Acquisition of 3-D arterial geometries and integration with computational fluid dynamics. Ultrasound Med Biol. 2009; 35: 2069-2083.
26. El-Hamamsy I, Yacoub MH. Cellular and molecular mechanisms of thoracic aortic aneurysms. Nat Rev Cardiol. 2009; 6: 771-786.
27. Markl M, Mikati I, Carr J, McCarthy P, Malaisrie SC. Three-dimensional blood flow alterations after transcatheter aortic valve implantation. Circulation. 2012; 125: e573-575.
28. Smith CR, Leon MB, Mack MJ, et al. Transcatheter versus surgical aortic-valve replacement in high-risk patients. N Engl J Med. 2011; 364: 2187-2198.
29. Viscardi F, Vergara C, Antiga L, et al. Comparative finite element model analysis of ascending aortic flow in bicuspid and tricuspid aortic valve. Artif Organs. 2010; 34: 1114-1120.
30. Wentzel JJ, Corti R, Fayad ZA, et al. Does shear stress modulate both plaque progression and regression in the thoracic aorta? Human study using serial magnetic resonance imaging. J Am Coll Cardiol. 2005; 45: 846-854.
31. Malek AM, Alper SL, Izumo S. Hemodynamic shear stress and its role in atherosclerosis. JAMA. 1999; 282: 2035-2042.
32. Elefteriades JA. Thoracic aortic aneurysm: reading the enemy's playbook. Curr Probl Cardiol. 2008; 33: 203-277.
33. Nicosia MA, Cochran RP, Einstein DR, Rutland CJ, Kunzelman KS. A coupled fluid-structure finite element model of the aortic valve and root. J Heart Valve Dis. 2003; 12: 781-789.
34. Morsi YS, Yang WW, Wong CS, Das S. Transient fluid-structure coupling for simulation of a trileaflet heart valve using weak coupling. J Artif Organs. 2007; 10: 96-103.
35. Sabbah HN, Stein PD. Fluid dynamic stresses in the region of a porcine bioprosthetic valve. Henry Ford Hosp Med J. 1982; 30: 134-138.
36. Bluestein D, Rambod E, Gharib M. Vortex shedding as a mechanism for free emboli formation in mechanical heart valves. J Biomech Eng. 2000; 122: 125-134.
37. Bluestein D, Li YM, Krukenkamp IB. Free emboli formation in the wake of bi-leaflet mechanical heart valves and the effects of implantation techniques. J Biomech. 2002; 35: 1533-1540.
38. Kaufmann TA, Linde T, Cuenca-Navalon E, et al. Transient, three-dimensional flow field simulation through a mechanical, trileaflet heart valve prosthesis. ASAIO J. 2011; 57: 278-282.
39. Grbic S, Mansi T, Ionasec R, et al. Image-based computational models for TAVI planning: from CT images to implant deployment. Med Image Comput Comput Assist Interv. 2013; 16: 395-402.
40. Schoenhagen P, Hill A, Kelley T, Popovic Z, Halliburton SS. In vivo imaging and computational analysis of the aortic root. Application in clinical research and design of transcatheter aortic valve systems. J Cardiovasc Transl Res. 2011; 4: 459-469.
41. Jin S, Oshinski J, Giddens DP. Effects of wall motion and compliance on flow patterns in the ascending aorta. J Biomech Eng. 2003; 125: 347-354.
42. Theodorakakos A, Gavaises M, Andriotis A, et al. Simulation of cardiac motion on non-Newtonian, pulsating flow development in the human left anterior descending coronary artery. Phys Med Biol. 2008; 53: 4875-4892.
43. Scharfschwerdt M, Meyer-Saraei R, Schmidtke C, Sievers HH. Hemodynamics of the Edwards Sapien XT transcatheter heart valve in noncircular aortic annuli. J Thorac Cardiovasc Surg. 2014; 148: 126-132.